Available online at www.sciencedirect.com
ScienceDirect
Journal of Catalysis 249 (2007) 174–184
JOURNAL OF CATALYSIS
www.elsevier.com/locate/jcat

CO dissociation on clean and hydrogen precovered Fe(111) surfaces

Chun-Fang Huo [a], Jun Ren [a], Yong-Wang Li [a], Jianguo Wang [a], Haijun Jiao [a,b,*]

[a] *State Key Laboratory of Coal Conversion, Institute of Coal Chemistry, Chinese Academy of Sciences, Taiyuan 030001, PR China*
[b] *Leibniz-Institut für Katalyse e.V. an der Universität Rostock, Albert-Einstein-Strasse 29a, 18059 Rostock, Germany*

Received 8 December 2006; revised 16 April 2007; accepted 21 April 2007

Available online 5 June 2007

Abstract

Spin-polarized density functional theory calculations were performed to investigate CO dissociation on clean and hydrogen precovered Fe(111) at 1/3 monolayer coverage. On clean Fe(111), the adsorbed CO first diffuses from the shallow-hollow site to the bridge-like site by elevating 0.20 eV in energy, and then dissociates into C and O atoms by overcoming a barrier of 1.53 eV. Interestingly, the CO dissociation process is accelerated in the presence of H_2 via intermediate CHO_{ads} ($CO_{ads} + 2H_{ads} \rightarrow CHO_{ads} + H_{ads} \rightarrow CH_{ads} + O_{ads} + H_{ads}$). This stepwise path is kinetically more favored with the lowest barrier of 1.17 eV. In contrast, the previously suggested paths, $CO_{ads} + 2H_{ads} \rightarrow C_{ads} + O_{ads} + 2H_{ads}$ and $CO_{ads} + 2H_{ads} \rightarrow C_{ads} + OH_{ads} + H_{ads}$, are not competitive due to higher barriers (1.76 and 1.79 eV, respectively). The activity of different low-index Fe surfaces toward CO is also compared.

Keywords: DFT; CO dissociation; Iron surfaces

1. Introduction

The interaction of CO with transition metal surfaces is of great fundamental and practical importance in many catalytic processes, including Fischer–Tropsch (FT) synthesis and methanation [1–3]. For iron-based catalysts, the FT reactivity is associated with the reducibility of iron oxides, the reoxidation of iron metal, and the reduction of iron carbides in connection with the coexistence of metal, oxide, and carbide phases [4,5]. Therefore, the reaction mechanism is extremely complicated [6]. It is believed that the adsorbed CO first dissociates into surface C and O ($CO_{ads} \rightarrow C_{ads} + O_{ads}$), which react with the dissociatively adsorbed H to form surface CH_x and OH_y ($C_{ads} + xH_{ads} \rightarrow CH_{x,ads}$, $O_{ads} + yH_{ads} \rightarrow OH_{y,ads}$) [7,8]. Consequently, considerable attention has been paid to the CO/Fe and (CO + H_2)/Fe systems [4–11]. However, most experimental and theoretical studies focused on the densely packed Fe(110) [12–18] and Fe(100) [15,19–31] surfaces. Only a few investigations have explored the very open Fe(111) surface, and the process for CO dissociation on Fe(111) remains unclear.

A thermal desorption spectroscopy (TDS) and high resolution electron energy loss spectroscopy (HREELS) study by Seip et al. [32] showed three molecular CO adsorption states on Fe(111), distinguished by their characteristic C–O stretch frequencies (ν_{C-O}): *state a* ($\nu_{C-O} = 1500\ cm^{-1}$), *state b* ($\nu_{C-O} = 1815\ cm^{-1}$), and *state c* ($\nu_{C-O} = 2000\ cm^{-1}$). Based on these, Seip et al. [32] further identified *state a* as the deep-hollow (dh) site (bonded to the exposed third-layer Fe atom), *state b* as the shallow-hollow (sh) site (bonded to the exposed second-layer Fe atom), and *state c* as the on-top site (bonded to the first-layer Fe atom). The subsequent HREELS study by Bartosch et al. [33] resolved the broad *state a* in two distinct peaks: *state* a_1 ($\nu_{C-O} = 1325$–$1485\ cm^{-1}$) and *state* a_2 ($\nu_{C-O} = 1520$–$1575\ cm^{-1}$). They found that *state* a_1 is formed primarily at low coverage but can be converted to *state* a_2 at high coverage when the on-top site becomes occupied.

In addition, Seip et al. [32] concluded that CO dissociation occurs only through the sh site (*state b*) regardless of coverage, whereas Bartosch et al. [33] suggested that *state* a_1 (dh site) dissociates directly, but it can convert to *state b* (sh site) before dissociation. Using temperature-programmed des-

* Corresponding author. Fax: +49 (0) 381/1281 5000.
E-mail address: haijun.jiao@catalysis.de (H. Jiao).

0021-9517/$ – see front matter
doi:10.1016/j.jcat.2007.04.018

orption (TPD) and time-resolved electron energy loss spectroscopy (TREELS), Whitman et al. [34] studied the kinetics of CO adsorption and reaction on Fe(111) and found that the site occupancy is highly temperature- and coverage-dependent. CO dissociation proceeds from the sh site at about 300 K. At low monolayer (ML) coverage (0.195 ML), the dissociation reaction occurs with $E = 0.9 \pm 0.2$ eV and $\nu_1 = 10^{11\pm2}/\mathrm{s}$. The resulting surface C and O atoms desorb recombinatively at about 760 K with $E \approx 2.1$ eV and $\nu_1 \approx 0.1\ \mathrm{cm}^2/\mathrm{s}$. At higher coverage (0.312 ML), in addition to dissociation, some of the adsorbed CO in the sh site desorbs with $E \approx 1.4$ eV and $\nu_1 \approx 10^{17}/\mathrm{s}$.

Based on atom superposition and molecular orbital theory, Mehandru and Anderson [16] studied the binding and orientation of CO on Fe(111) using a three-layer, 27-atom cluster model. They calculated that CO adsorbs in the order di-σ bridge > on-top > shallow-hollow > deep-hollow, in disagreement with the experimental order of shallow-hollow > deep-hollow > on-top reported by Seip et al. [32] and Bartosch et al. [33]. It is likely that the level of the theory and the model used by Mehandru and Anderson were insufficient to give a quantitative (or even qualitative) description of the process.

More recently, a detailed study of CO adsorption on Fe(111) performed at the level of density functional theory (DFT) [35] found that CO site occupancies depend on the coverage. At low coverage (1/3 and 1/2 ML), the sh adsorption site is the most stable site, whereas the sh and the bridge (br) sites are equally favored at 1 ML. In contrast, bent on-top and triply capping adsorptions are the most favored forms at very high coverage (2 ML).

It is well known that the surface carbon from CO dissociation may stay on the surface or lead to carburization of the catalyst. The rate of carburization reaction is faster in the presence of H_2 than in the absence of H_2 [36]. A study of CO/H_2 reaction on a Ni catalyst by Ho and Harriott [37] proposed the following hydrogen-assisted CO dissociation reactions:

$$\mathrm{CO_{ads}} + \mathrm{H_{ads}} \rightarrow \mathrm{COH_{ads}} \tag{1}$$

and

$$\mathrm{COH_{ads}} + \mathrm{H_{ads}} \rightarrow \mathrm{C_{ads}} + \mathrm{H_2O_{(g)}}. \tag{2}$$

But this mechanism was ruled out by Bianchi and Bennett [38] on the Fe–Al_2O_3 catalytic system, because $H_2O_{(g)}$ was not detected in the effluent during the reaction. By determining the amount of CO_2 formed during contact of the feed gas (10% CO + 1% H_2 + 89% He and 10% CO + 90% He) with the surface or the quantity of CH_4 produced by etching the spent catalyst with pure H_2, Bianchi and Bennett proposed an alternative mechanism,

$$\mathrm{H_2} \rightarrow 2\mathrm{H_{ads}} \tag{3}$$

and

$$\mathrm{CO_{ads}} + \mathrm{H_{ads}} \rightarrow \mathrm{C_{ads}} + \mathrm{OH_{ads}}. \tag{4}$$

Here we present a systematic DFT study of CO dissociation on clean and hydrogen-precovered Fe(111) surfaces. The aim is to describe the changes of the surface structure and energy during CO dissociation, and also to elucidate the role of hydrogen in the mechanism of FT synthesis.

2. Computational details

2.1. Methods

All calculations were performed at the DFT level with the CASTEP program [39,40] in the Materials studio of Accelry Inc. For geometry optimizations, the exchange and correlation energies were calculated using the Perdew, Burke, and Ernzerhof (PBE) functional [41] within the generalized gradient approximation (GGA) [42]. The electron–ion interactions were described by ultrasoft pseudopotentials (USPPs) [43] with the plane-wave basis set cutoff at 340 eV. A Fermi smearing of 0.1 eV was used to evaluate occupancy numbers. Because of its significant effect on the adsorption energies for magnetic systems [44–46], spin polarization was included in the calculations for the system with Fe. The convergence criteria for structure optimization and energy calculation were set to MEDIUM quality with the tolerance for SCF, energy, maximum force, and maximum displacement of 2.0×10^{-6} eV/atom, 2.0×10^{-5} eV/atom, 0.05 eV/Å and 2.0×10^{-3} Å, respectively. The linear synchronous transit (LST)/optimization method [47] was used to locate the transition states for CO dissociation. The transition state structure was estimated by a linear synchronous search from reactant and product, followed by a conjugate gradient energy minimization in the directions conjugating to the reaction pathway.

It should be noted that the PBE functional can give reliable optimized geometry but tends to overestimate the adsorption energies by 0.2–0.6 eV. Based on this finding, a revised PBE (RPBE) method was developed [48]. The RPBE systematically improves the atomization energies for a large database of small molecules and the chemisorption energies of atoms and molecules on a transition-metal surface. Therefore, we further carried out RPBE single-point calculations on the PBE-optimized geometries. In the following sections, we use the RPBE energies for discussion and provide the PBE values for comparison.

2.2. Models

Fe(111) has a step-like or defect-like surface with atoms of both the second and the third layers exposed. The top and side views are shown in Fig. 1; the first, second, and third iron layers are labeled Fe1, Fe2, and Fe3, respectively. Both experimental [49] and our previous DFT [35,50] studies verified that the very open structure of the clean Fe(111) surface exhibits significant multilayer relaxation. For modeling Fe(111), a slab with seven iron layers was used, in which the top three layers were allowed to relax, while the bottom four layers were fixed in their bulk position (3Fe/4Fe) to represent the semi-infinite bulk crystal beneath the surface. All adsorbates were put on only one side of the slab. The free CO or H_2 molecule was placed in a 10 Å cubic box to minimize the interaction of neighboring molecules, and the equilibrium bond length of CO or H_2 is predicted to be 1.144 or 0.753 Å (comparable to the experimental values of 1.128 or 0.741 Å [51]). The energy of an isolated C or O atom was computed in its ^{3}P ground state (as indicated by the population analysis, i.e., C: $2s^2 2p^2$ or O: $2s^2 2p^4$) by putting a C or

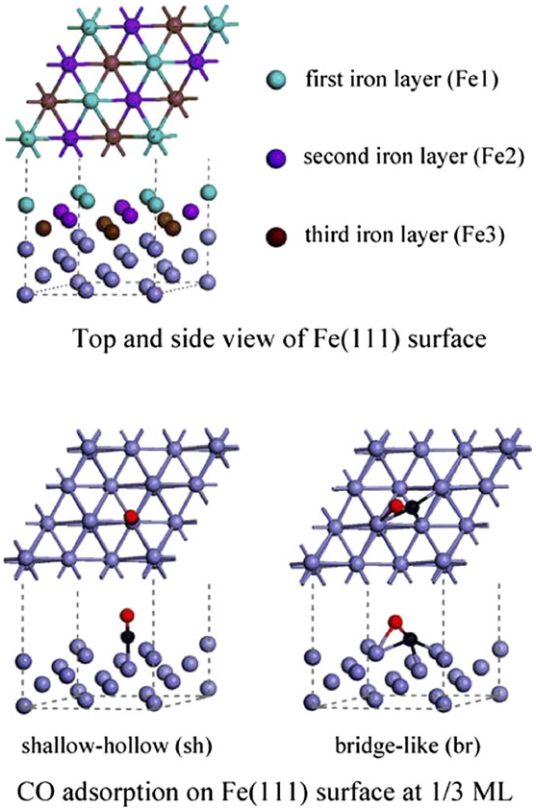

Fig. 1. Top and side view of Fe(111) as well as CO adsorption configurations at 1/3 ML (blue: Fe atom, black: C atom, red: O atom). (For interpretation of the references to color in this figure legend, the reader is referred to the web version of this article.)

O atom in a 10 Å cubic box and performing a spin-polarized single-point calculation.

Under the typical FT reaction conditions of 300–350 °C (or 220–280 °C) and 1.5–2.5 MPa [52], all adsorption sites of the catalyst surfaces became occupied. Experimental studies [34,53] showed that the saturation coverage of CO adsorbed on the Fe(111) surface is in the range of 1.3–1.5 ML, depending on the temperatures. The saturation coverage of dissociated CO on the Fe(111) surface is 1/4 of that of molecular CO; therefore, a $p(\sqrt{3}\times\sqrt{3})$ unit cell with one adsorbed molecular CO was used to investigate the CO dissociation process, corresponding to 1/3 ML. The k-point mesh was $(3\times3\times1)$. To validate the methods and models, the convergence of the results was checked by increasing the cutoff energy (400 eV), the number of the slab (3Fe/5Fe) and relaxed layers (4Fe/3Fe), and the number of k-points $(4\times4\times1)$. The changes of the CO adsorption energy are found to be 0.03, 0.02, 0.04, and 0.03 eV, respectively.

The adsorption energy is defined as $E_{ads} = E(\text{adsorbates/slab}) - [E(\text{slab}) + E(\text{adsorbates})]$, where E(adsorbates/slab) is the total energy of the slab with adsorbates, E(slab) is the total energy of the corresponding bare Fe slab, and E(adsorbates) is the total energy of free adsorbates. Thus, the more negative the E_{ads}, the stronger the adsorption. The coverage (θ) is defined as the number of the adsorbates over the number of the first-layer Fe atoms.

Table 1
Adsorption energies (E_{ads}, eV) and calculated bond lengths (d, Å) as well as net charges of CO for CO adsorption on Fe(111) at 1/3 ML

	E_{ads}[a]	d_{C-O}[a]	d_{C-Fe1}[a] [d_{O-Fe1}][a]	d_{C-Fe2}[a]	q_{CO}
CO (sh)	−2.08[b] (−2.45)	1.191		1.749	−0.46
CO (br)	−1.88[b] (−2.35)	1.239	1.996 2.134 [2.175]	1.841	−0.64
CO (top)	−1.35[b] (−1.65)	1.167	1.791		−0.24

[a] Values are derived from the PBE functional.
[b] Values are derived from the RPBE functional.

3. Results and discussion

3.1. CO adsorption on Fe(111) at 1/3 ML

Our previous study [35] showed that the CO adsorption sites and their relative stabilities on Fe(111) are highly dependent on the coverage. At 1/3 ML, the most favored adsorption site for CO is the sh site, followed by the br site with an energy difference of 0.20 eV. The on-top site is not competitive, as indicated by the low adsorption energy of −1.35 eV with respect to that of −2.08 eV for the sh site (Table 1).

As shown in Fig. 1 and Table 1, at the sh site, CO bonds uprightly on Fe2, and the C–O bond is elongated to 1.191 Å (1.144 Å for free CO). However, at the br site, CO interacts with Fe via both the carbon (in μ^3 form) and oxygen (in μ^1 form) atoms and tilts away from the surface normal by 40.2°. It is interesting to note that the C–O bond (1.239 Å) in this tilted form is more activated, although the br site is slightly less stable (by 0.20 eV) than the sh site. Because a lying-down CO orientation has been proposed as the precursor state for CO dissociation in FT catalysis [3,54,55], our succeeding discussions focus mainly on CO dissociation from the br site.

3.2. C and O adsorption on Fe(111) at 1/3 ML

To investigate the CO dissociation process, we first need to know the individual bonding natures of C/Fe(111) and O/Fe(111) systems. All possible adsorption sites were considered at 1/3 ML, and only four stable sites for individually adsorbed C and O (**1–4**) were located: the on-top site (**1**), the top-shallow bridge (tsb) site (**2**), the quasi-fourfold (qff) site (**3**), and the quasi-plane (qp) site (**4**) (Fig. 2). The corresponding adsorption energies and calculated bond parameters are given in Table 2.

The adsorption energies in Table 2 indicate that C atoms bind strongly with the Fe(111) surface. At 1/3 ML, the C atom prefers high coordination sites of the qff (**3/C**) and qp (**4/C**) sites with adsorption energies of −7.27 and −7.22 eV, respectively. In **4/C** (qp), the C atom interacts with one Fe1, two Fe2, one Fe3 and one additional Fe4 in μ^5 coordination form and embeds into the Fe(111) surface by 0.84 Å. Similar trends in site preference in high coordination have been found on other low-index Fe surfaces [i.e., the long-bridge site on Fe(110) and

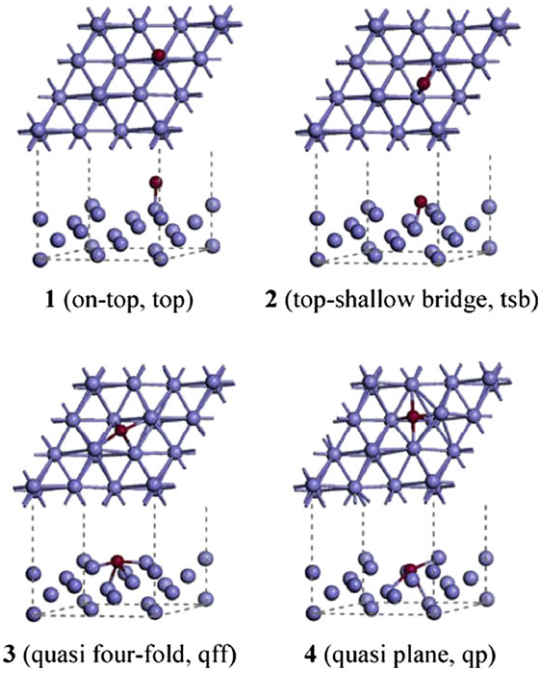

Fig. 2. C or O atom adsorption sites on Fe(111) at 1/3 ML (blue: Fe atom, dark red: C or O atom). (For interpretation of the references to color in this figure legend, the reader is referred to the web version of this article.)

Table 2
Adsorption energies (E_{ads}, eV) and calculated bond lengths (d, Å) for C and O adsorption on Fe(111) at 1/3 ML

No.	E_{ads} [a]	$d_{C–Fe1}$	$d_{C–Fe2}$	$d_{C–Fe3}$	$d_{C–Fe4}$
1/C (top)	−4.63	1.585			
	(−4.92)				
2/C (tsb)	−6.26	1.707	1.769		
	(−6.70)				
3/C (qff)	−7.27	1.890	1.818	1.951	
	(−7.80)	1.890			
4/C (qp)	−7.22	1.784	1.925	1.792	2.246
	(−7.74)		1.920		
		$d_{O–Fe1}$	$d_{O–Fe2}$	$d_{O–Fe3}$	
1/O (top)	−4.44	1.617			
	(−4.75)				
2/O (tsb)	−5.24	1.836	1.781		
	(−5.63)				
3/O (qff)	−5.42	1.963	1.834	2.249	
	(−5.87)	1.964			
4/O (qp)	−4.93	1.872	2.134	1.955	
	(−5.33)		2.191		

[a] Values in parentheses are derived from the PBE functional.

the fourfold hollow (ffh) site on Fe(100)]. In addition, the adsorption energy changes significantly as the C atom coverage increases on Fe(110) (−7.77 eV at 1/4 ML and −7.06 eV at 1/2 ML), but only slightly on Fe(100) (−8.24 eV at 1/4 ML and −8.28 eV at 1/2 ML) [56]. Comparing the PBE adsorption energies on Fe(111) (−7.80 for qff and −7.74 eV for qp at 1/3 ML) with those on Fe(110) and Fe(100) shows that C atoms bind most strongly on Fe(100), followed by Fe(111) and Fe(110). Furthermore, C atoms remain on the surfaces on Fe(110) and Fe(100).

In contrast to the C atom, the O atom favors the gff (**3/O**) and the tsb (**2/O**) sites on Fe(111), with adsorption energies of −5.42 and −5.24 eV, respectively. In these cases, the O atom is 0.43 or 0.85 Å over the surface. The adsorption of O atom on Fe(110) and Fe(100) was studied by Błoński et al. using the PW91 functional [57]. They found that at 1/4 ML, the most stable adsorption sites were the long-bridge site on Fe(110) and the ffh site on Fe(100), with respective adsorption energies of −3.28 and −3.41 eV. These energy data suggest that O atoms bind most strongly on Fe(111), followed by Fe(100) and Fe(110).

3.3. C and O coadsorption on Fe(111) at 1/3 ML

Because C atom adsorption is stronger than O atom adsorption on Fe(111) (−7.27 vs 5.42 eV), the C atom will occupy the preferred site over the O atom during the CO dissociation process. For the C atom preadsorbed on the qff site (**3/C**) and the qp site (**4/C**) sites, all possible adsorption sites for O atom were considered, and only seven stable C and O coadsorption modes (**5–11**) were found, as shown in Fig. 3. The adsorption energies and calculated bond parameters are given in Table 3.

As shown in Fig. 3, **5–8** correspond to a C atom preadsorbed on the qff site. In **5**, both C and O atoms reside at the qff sites and share one Fe1 in a linear way (Fe1-C-Fe1-O-Fe1), and the computed CO dissociative adsorption energy is −1.86 eV. In **6**, both C and O atoms occupy the qff sites and share one Fe1 in a zigzag way, and the computed CO dissociative adsorption energy is −1.85 eV, very close to that of **5**. As expected, **7** with a C atom at the qff site and an O atom at the tsb site has slightly more energy (−1.72 eV). **8**, with a C atom at the qff site and a O atom at the on-top site has much more energy (−0.60 eV) and thus is not competitive. When initially put at the qp site, the O atom relaxes to the qff site, leading to **5** or **6**.

For a C atom preadsorbed on the qp site, only three C and O co-adsorbed modes (**9–11**) are located, with an O atom occupying the qff site in μ^4 form (**9**) or in μ^3 form (**10**) and the on-top site (**11**), respectively. When initially put at the tsb site or the qp site, the O atom relaxes to the qff site, leading to **9** or **10**. As expected, **9** has a similar CO dissociative adsorption energy (−1.75 eV) to **5**, whereas **11** has a lower CO dissociative adsorption energy of −0.51 eV, comparable with that of **8** (−0.60 eV). However, a much higher CO dissociative adsorption energy is computed for **10** (−2.24 eV). To elucidate this quantity, it is necessary to value the difference (ΔE_{ads}) in adsorption energy between C and O coadsorption [E_{ads}(C/O), with respect to atomic C and O] and the sum of C and O individual adsorptions on the same site as in coadsorption [E_{ads}(C) + E_{ads}(O)]. The negative energy differences of −0.04 to −0.52 eV (Table 3) indicate that there are no repulsive interactions between the adsorbed C and O atoms in **5–7**, **9**, and **10**. In addition, the local surface–atom coordination of the adsorption site may be responsible for the enhanced stability of **10**. As shown in Fig. 3, C and O coadsorption leads to a significant reconstruction of Fe(111) in **10**. At the adsorption region, two Fe–Fe bonds are broken, as indicated by the long distances of 3.106 Å for Fe1–Fe2 and 3.196 Å for Fe1–Fe3 [compared with 2.443 and 2.735 Å in the pure Fe(111) slab]. As a consequence, the unsaturated degree of the C and O shared Fe1 atom

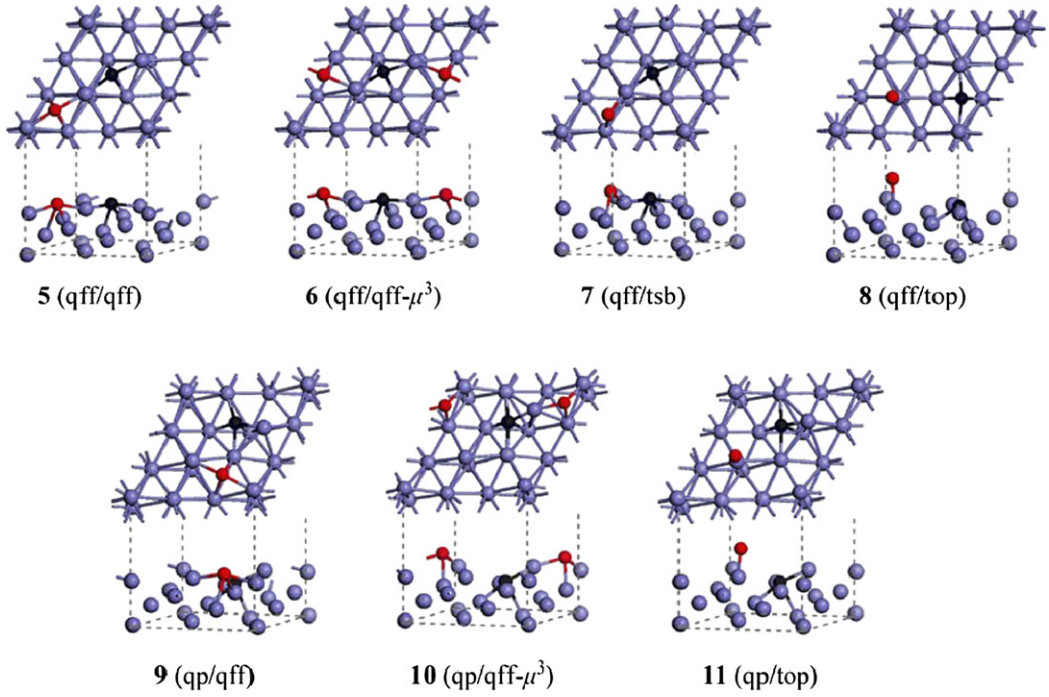

Fig. 3. Configurations of C/O co-adsorption on Fe(111) at 1/3 ML (blue: Fe atom, black: C atom, red: O atom). (For interpretation of the references to color in this figure legend, the reader is referred to the web version of this article.)

Table 3
Adsorption energies (E_{ads}, eV) and calculated bond lengths (d, Å) for C/O co-adsorption on Fe(111) at 1/3 ML

No.	Mode (C/O)	E_{ads} [a]	E_{ads}(C/O) [b]	ΔE_{ads} [c]	$d_{C–Fe1}$ [$d_{O–Fe1}$]	$d_{C–Fe2}$ [$d_{O–Fe2}$]	$d_{C–Fe3}$ [$d_{O–Fe3}$]	$d_{C–Fe4}$
5	qff/qff	−1.86	−12.79	−0.10	1.916, 1.887	1.814	1.987	
		(−2.53)	(−13.74)	(−0.07)	[1.956, 1.991]	[1.843]	[2.242]	
6	qff/qff-μ^3	−1.85	−12.78	−0.09	1.881, 1.892	1.826	1.971	
		(−2.48)	(−13.68)	(−0.01)	[1.968, 1.955]	[1.868]		
7	qff/tsb	−1.72	−12.65	−0.14	1.887, 1.860	1.831	1.965	
		(−2.31)	(−13.52)	(−0.09)	[1.817]	[1.792]		
8	qff/top	−0.60	−11.53	0.18	1.885, 1.886	1.928	1.808	
		(−1.16)	(−12.36)	(0.19)	[1.619]			
9	qp/qff	−1.75	−12.68	−0.04	1.828	1.875, 1.932	1.862	2.093
		(−2.42)	(−13.62)	(−0.01)	[1.968, 1.963]	[1.883]	[2.147]	
10	qp/qff-μ^3	−2.24	−13.16	−0.52	1.832	1.939, 1.910	1.816	2.191
		(−2.87)	(−14.07)	(−0.46)	[1.900, 1.901]	[1.916]		
11	qp/top	−0.51	−11.44	0.22	1.781	1.931, 1.933	1.788	2.215
		(−1.33)	(−12.53)	(−0.04)	[1.632]			

[a] Dissociative adsorption energies with respect to gas-phase CO; values in parentheses are derived from the PBE functional.
[b] Adsorption energies with respect to atomic C and O.
[c] $\Delta E_{ads} = E_{ads}(C/O) - [E_{ads}(C) + E_{ads}(O)]$.

is increased, and thus the strengths of the chemisorption bonds are enhanced.

3.4. CO dissociation on clean Fe(111) at 1/3 ML

Based on CO adsorption and C/O coadsorption, CO dissociation from the br site was examined first, and five possible paths (br → **5, 6, 7, 9, 10**) were mapped out. The energy data in Table 4 clearly show that the path br → **TS(br/10)** → **10** is more favored both kinetically and thermodynamically. This reaction is exothermic by −0.36 eV and has an energy barrier of 1.53 eV. In the transition state **TS(br/10)**, the C–O bond is very elongated (2.002 Å), with the O atom close to a bridge site (Fig. 4). This type of transition state is quite common for CO dissociation on transition metal surfaces [18,28,58]. Also note that the C atom embeds into the Fe(111) surface by 1.13 Å, whereas the O atom is 0.92 Å above the surface after dissociation (**10** in Fig. 3), in line with the Raman ellipsometry spectroscopy observation [9]. Watanabe and Kadowaki found that CO dissociation produces a thin Fe_3O_4 layer on the Fe surface, which occludes large numbers of C atoms in the Fe phase.

Because CO prefers the sh site over the br site by 0.20 eV, diffusion and dissociation from this site also were examined. CO diffusion from the sh site to the br site has no additional bar-

Table 4
Activation and reaction energies (E_a and ΔE_{re}, eV) for CO dissociation on clean Fe(111) at 1/3 ML as well as calculated bond lengths (d, Å) for transition states

	E_a[a]	ΔE_{re}[a]	d_{C-O}	d_{C-Fe1} [d_{O-Fe1}]	d_{C-Fe2} [d_{O-Fe2}]	d_{C-Fe3}
TS(br/5)	2.22	0.02	1.862	1.822, 1.930	1.828	2.132
	(2.15)	(−0.18)		[1.692]		
TS(br/6)	2.15	0.03	2.019	1.855, 1.923	1.805	1.960
	(2.09)	(−0.13)		[1.707]		
TS(br/7)	2.52	0.16	1.990	1.975, 1.926	1.778	
	(2.47)	(0.04)		[1.669]		
TS(br/9)	2.06	0.13	1.841	1.821	1.939	1.815
	(1.94)	(−0.07)		[1.878]	[1.954]	
TS(br/10)	1.53	−0.36	2.002	2.309, 1.882	1.895	1.892
	(1.39)	(−0.52)		[1.835]	[1.884]	
TS(sh/10)	2.71	−0.16	1.992	2.181, 1.793	1.859	
	(2.64)	(−0.42)		[1.719]		
TS(sh/br)	0.19	0.20	1.215	2.188, 2.231	1.783	
	(0.15)	(0.10)		[2.481]		

[a] Values in parentheses are derived from the PBE functional.

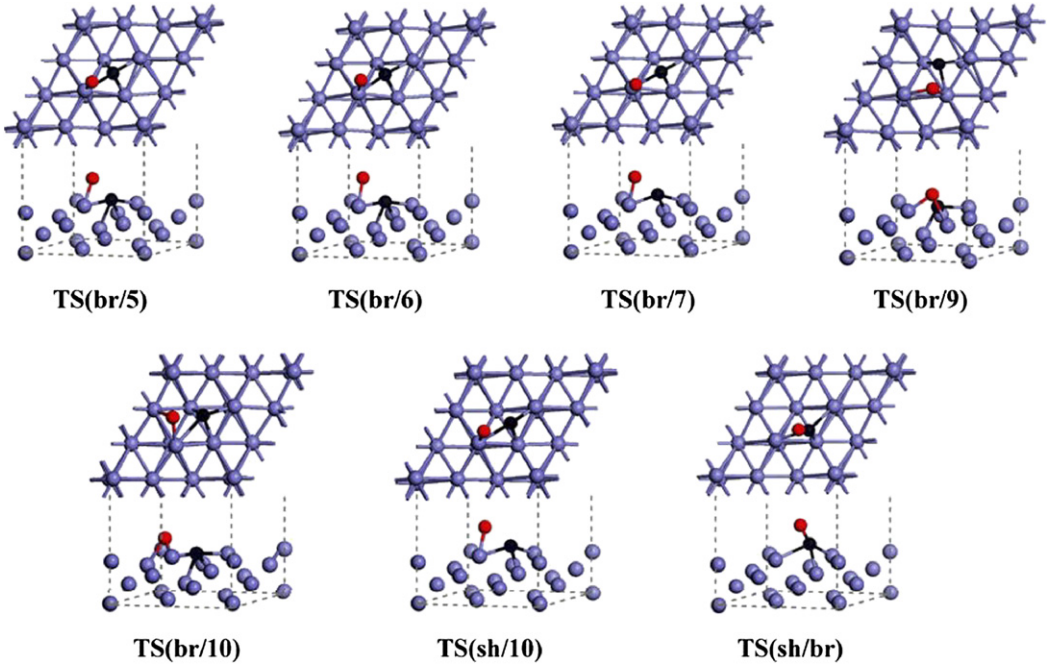

Fig. 4. Configurations of transition states for CO dissociation on clean Fe(111) at 1/3 ML (blue: Fe atom, black: C atom, red: O atom). (For interpretation of the references to color in this figure legend, the reader is referred to the web version of this article.)

rier, whereas CO dissociation directly from the sh site leading to **10** needs to overcome a high barrier of 2.71 eV. Therefore, the path of diffusion followed by dissociation at the br site is favored, and the dissociation directly at the sh site is not competitive.

An early temperature-programmed desorption (TPD) and time-resolved electron energy loss spectroscopy (TREELS) study by Whitman et al. [34] determined the kinetic data of CO adsorption and reaction on Fe(111). It was observed that at 0.312 ML, in addition to dissociation, some of the adsorbed CO in the sh site desorbs with $E \approx 1.4$ eV. Both experimental [25,59] and theoretical [29] studies have shown that the adsorption energy of CO is decreased by the presence of carbon or oxygen on Fe surface, and thus the analysis of the desorption data will yield not the heat of adsorption of CO molecules in the corresponding state when some of CO dissociate, but rather the apparent activation energy for dissociation. This suggests that the activation energy for CO dissociation at 1/3 ML should be close to 1.4 eV, whereas the higher adsorption energy for CO in the sh site is desired. Considering that the inherent accuracy of the DFT calculations is of the order 0.2–0.3 eV [48,60], our calculated values of 1.53 eV for the apparent activation energy of CO dissociation from the br site and 2.08 eV for the adsorption energy of CO in the sh site at 1/3 ML are reasonable. Furthermore, the predicted value for the recombinative desorption of surface C and O atoms is 2.24 eV, in agreement with the experimental value of 2.1 eV [34].

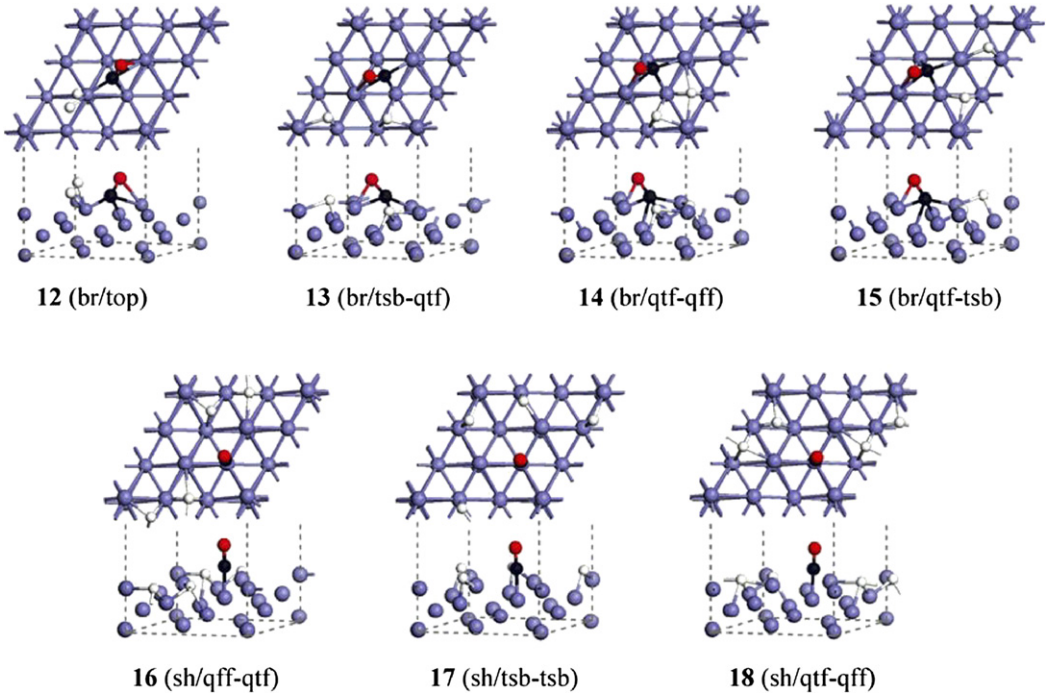

Fig. 5. Configurations of CO/H_2 co-adsorption on Fe(111) (blue: Fe atom, black: C atom, red: O atom, white: H atom). (For interpretation of the references to color in this figure legend, the reader is referred to the web version of this article.)

Table 5
Adsorption energies (E_{ads}, eV) and calculated bond lengths (d, Å) as well as net charges of CO for CO/H_2 co-adsorption on Fe(111)

No.	Mode (CO/H_2)	E_{ads}[a]	d_{C-O}	d_{C-Fe1} [d_{O-Fe1}]	d_{C-Fe2}	d_{C-Fe3}	d_{H-Fe1} a/[b]	d_{H-Fe2} a/[b]	d_{H-Fe3} a/[b]	q_{CO}
12	br/top	−2.22 (−3.02)	1.249	2.220, 1.845 [2.036]	1.929		1.567 [1.589]			−0.63
13	br/tsb-qtf	−2.71 (−3.53)	1.242	1.938, 2.201 [2.098]	1.870		1.950 [1.787]	1.616 [1.709]	[1.765]	−0.63
14	br/qtf-qff	−2.35 (−3.24)	1.258	1.981, 2.108 [2.114]	1.962	2.070	1.851 [2.067, 1.944]	1.684 [1.689]	1.798 [1.795]	−0.71
15	br/qtf-tsb	−2.57 (−3.41)	1.258	1.975, 2.093 [2.077]	1.935	2.129	1.853 [1.811]	1.696 [1.640]	1.792	−0.72
16	sh/qff-qtf	−3.00 (−3.73)	1.191		1.749		2.076, 1.930 [1.846]	1.648 [1.655]	1.924 [1.900]	−0.45
17	sh/tsb-tsb	−3.15 (−3.80)	1.190		1.748		1.853 [1.863]	1.607 [1.604]		−0.45
18	sh/qtf-qff	−3.00 (−3.73)	1.191		1.748		1.846 [1.930, 2.090]	1.650 [1.648]	1.938 [1.922]	−0.46

[a] With respect to gas-phase CO and H_2; values in parentheses are derived from the PBE functional.

3.5. CO and H_2 coadsorption on Fe(111)

To understand the hydrogen-assisted CO dissociation process, the coadsorption of CO and H_2 with a H_2/CO ratio of 1/1 and CO preoccupied the br site was considered. Isotope-exchange experiments revealed the atomic nature of hydrogen held at the Fe(111) surface above 140 K [61]. Our previous DFT study [50] also indicated that the dissociation of hydrogen has no barrier. All possible adsorption sites for H_2 were examined, and only seven coadsorption forms (**12–18**) were found (Fig. 5). The adsorption energies and the calculated bond parameters are listed in Table 5.

Fig. 5 shows that the coadsorption of CO (1/3 ML) and H_2 (2/3 ML) on Fe(111) does not lead to any hydrogenation products. In **12**, CO resides at the br site and H_2 is activated on the on-top site. Note that we first put H_2 on the Fe1 of the O side, but the repulsive interaction between H_2 and CO shifts the O atom to the opposite Fe1 site, which means that O and H_2 do not share the same Fe1. As expected, this form has the lowest adsorption energy, −2.22 eV. In **13–15**, CO still occupies the br site, while H_2 dissociatively adsorbs on the tsb/qtf, qtf/qff, and qtf/tsb sites. These adsorption forms have moderate adsorption energies of −2.71, −2.35, and −2.57 eV, respectively. For **16–18**, the site occupancy of CO changes from the br site to the sh site to minimize the repulsive interactions between CO and H adatoms, and higher adsorption energies result (−3.00, −3.15, and −3.00 eV, respectively). For the net charges of the adsorbed CO (Table 5), no obvious changes

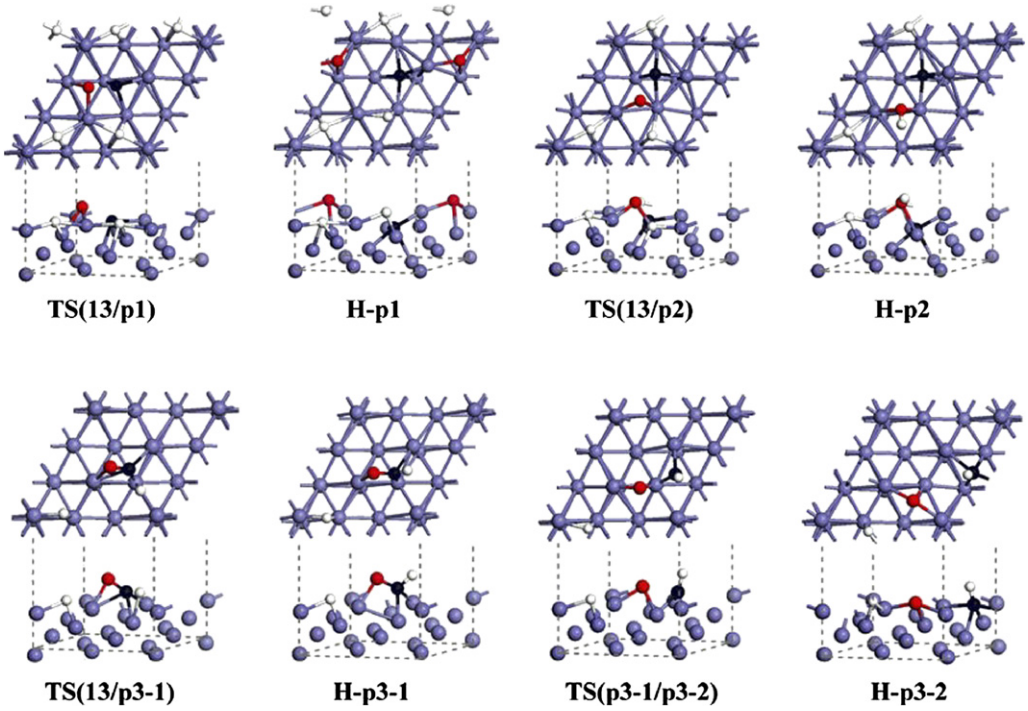

Fig. 6. Configurations of transition states and intermediates for CO dissociation on hydrogen precovered Fe(111) (blue: Fe atom, black: C atom, red: O atom, white: H atom). (For interpretation of the references to color in this figure legend, the reader is referred to the web version of this article.)

can be observed with respect to CO individual adsorption (Table 1).

Because adsorbed CO and H atom have high mobility on Fe(111) [50], and the br site favors CO dissociation, the following discussion about the hydrogen-assisted CO dissociation is based on **13**.

3.6. CO dissociation on hydrogen precovered Fe(111)

Taking **13** as the starting point, three possible paths for CO dissociation on a hydrogen-precovered Fe(111) surface can be conceived: (A) $CO_{ads} + 2H_{ads} \rightarrow C_{ads} + O_{ads} + 2H_{ads}$, (B) $CO_{ads} + 2H_{ads} \rightarrow C_{ads} + OH_{ads} + H_{ads}$, and (C) $CO_{ads} + 2H_{ads} \rightarrow CHO_{ads} + H_{ads}$; $CHO_{ads} + H_{ads} \rightarrow CH_{ads} + O_{ads} + H_{ads}$. The corresponding structures of all transition states and intermediates are depicted in Fig. 6, the calculated bond parameters are given in Table 6, and the energy profiles are presented in Fig. 7.

Path A is the elementary step of the widely accepted carbide mechanism for FT synthesis [7,8]. As shown in Fig. 6, path A (**13** → **TS(13/p1)** → **H-p1**) is very similar to the corresponding process (**br** → **TS(br/10)** → **10**) for CO dissociation on clean Fe(111) from the structural aspect (Figs. 2–4). However, rising from the repulsive interactions caused by the H adatoms, the direct CO dissociation path has a higher barrier of 1.76 eV under synthesis gas ($CO + H_2$) conditions.

For path B (proposed by Bianchi and Bennett [38]), the dissociation of the C–O bond is accompanied by formation of an O–H bond. As shown in Fig. 6, path B performs via transition state **TS(13/p2)**, leading to the intermediate **H-p2** with the dissociated C atom at the qp site and the OH species occupying the tsb site through an O atom. The main change in the early stage [from **13** to **TS(13/p2)**] is breakage of the C–O bond, whereas the O–H bond is formed during the late stage [from **TS(13/p2)** to **H-p2**]. As shown in Fig. 7, this path has a barrier of 1.79 eV, close to that of path A, and is endothermic by 0.43 eV.

Path C is a new proposed route for CO dissociation in the presence of H_2 that proceeds stepwise. First, the dissociatively adsorbed H atom migrates to the adsorbed CO, forming the CHO species. As illustrated in Fig. 6, this step occurs through the transition state **TS(13/p3-1)**, leading to intermediate **H-p3-1**, in which the CHO species interacts with the Fe(111) surface by the CO group occupying the adjacent tsb sites. It is noteworthy that migration of the H atom makes the C–O bond parallel to the Fe1–Fe2 bond and thus highly activated, as indicated by the long C–O distance of 1.297 Å (with respect to 1.239 Å for the bridge-like adsorbed CO and 1.144 Å for free CO). The energy profiles in Fig. 7 show that this H adatom migration process is endothermic by 0.57 eV, with a relatively low energy barrier of 0.99 eV. In the second step, the highly activated C–O bond is broken with formation of the key FTS intermediates, CH and O (**H-p3-1** → **TS(p3-1/p3-2)** → **H-p3-2**). In the corresponding transition state **TS(p3-1/p3-2)**, the C–O bond is elongated to 2.083 Å, with the O atom occupying the tsb site. This step is predicted to be exothermic by −0.82 eV and has an energy barrier of 1.17 eV. More importantly, the energy profiles in Fig. 7 clearly show that CO dissociation on hydrogen-precovered Fe(111) favors path C kinetically, with the lowest dissociation energy barrier of 1.17 eV. Paths A and B are not competitive and cannot occur under the present reaction conditions ($\theta_{CO} = 1/3$ ML and $H_2/CO = 1/1$).

Table 6
Calculated bond lengths (d, Å) for transition states and intermediates involved in the CO dissociation on hydrogen precovered Fe(111)

	d_{C-O}	d_{C-H} [d_{O-H}]	d_{C-Fe1} [d_{O-Fe1}]	d_{C-Fe2} [d_{O-Fe2}]	d_{C-Fe3}	d_{H-Fe1} a/[b]	d_{H-Fe2} a/[b]	d_{H-Fe3} a/[b]
			Path A: $CO_{ads} + 2H_{ads} \rightarrow C_{ads} + O_{ads} + 2H_{ads}$					
TS(13/p1)	1.859		1.916	1.973	1.735	1.909, 2.086	1.588	
			[1.974]	[1.912]		[1.964, 1.889]	[1.586]	[2.037]
H-p1			1.825	1.909, 1.936	1.814	1.909, 2.082	1.676	1.916
			[1.901, 1.904]	[1.903]		[1.804]	[1.619]	
			Path B: $CO_{ads} + 2H_{ads} \rightarrow C_{ads} + OH_{ads} + H_{ads}$					
TS(13/p2)	2.258		1.808	1.932, 1.880	1.863	2.047, 1.853	1.631	
		[2.323]	[1.724]	[1.949]		[1.691]	[1.751]	[1.682]
H-p2			1.770	1.965, 1.898	1.781	1.981, 1.967	1.624	
		[0.977]	[1.940]	[2.049]				
			Path C: $CO_{ads} + 2H_{ads} \rightarrow CHO_{ads} + H_{ads}$; $CHO_{ads} + H_{ads} \rightarrow CH_{ads} + O_{ads} + H_{ads}$					
TS(13/p3-1)	1.263	1.370	2.032, 2.291	1.848		1.885	1.872	
			[2.021]			[1.841]	[1.615]	
H-p3-1	1.297	1.116	2.249	1.863				
			[1.931]			[1.834]	[1.631]	
TS(p3-1/p3-2)	2.083	1.123	1.805	1.851				
			[1.892]	[1.932]		[1.904]	[1.677]	
H-p3-2		1.103	2.076, 1.978	1.889	1.991			
			[1.949, 1.976]	[1.851]		[1.732]	[1.656]	

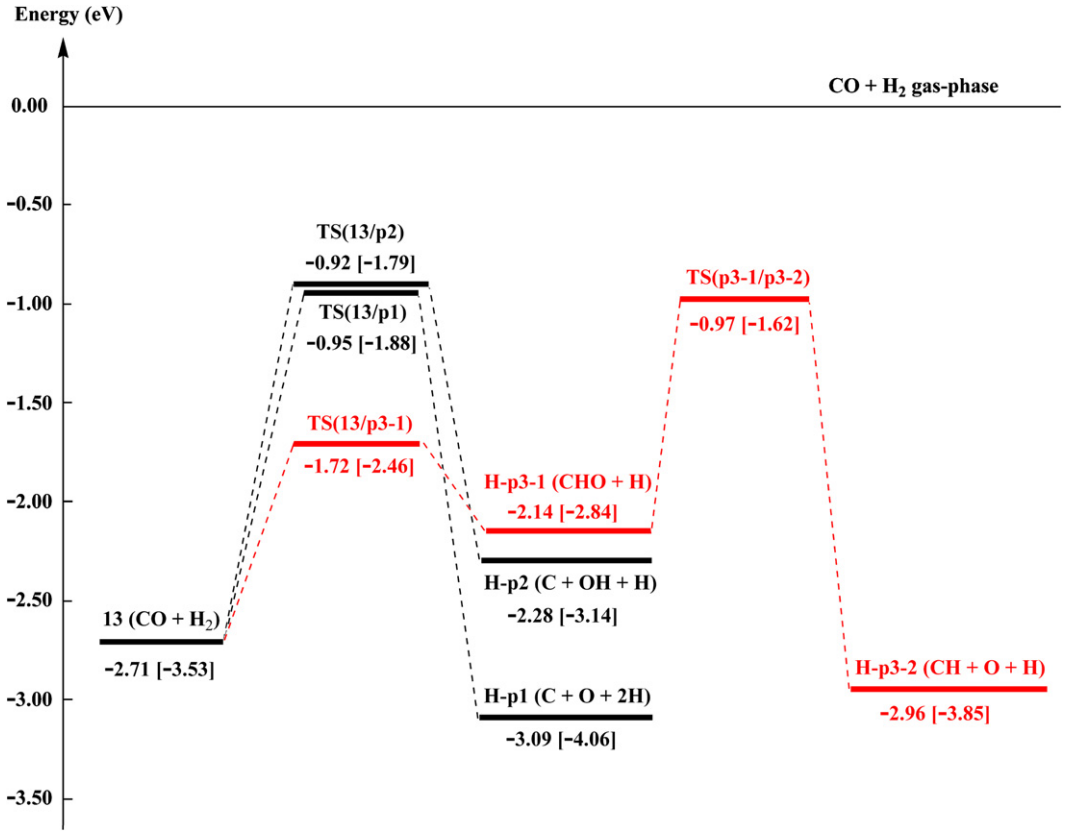

Fig. 7. Energy profiles (eV, values in parentheses are derived from the PBE functional) for CO dissociation on hydrogen precovered Fe(111).

3.7. Activity comparison of the low-index Fe surfaces

Based on our calculations, it is interesting to compare the activity of the low-index Fe surfaces toward CO. Fe(110) is the most closely packed and most stable surface of the body-centered cubic Fe. An experiment by Erley [13] suggested that CO prefers the on-top site at 1/4 ML, with a characteristic C–O stretching frequency of 1956 cm^{-1}. A recent DFT study by Jiang and Carter [18] predicted that CO dissociation on the on-top site at 1/4 ML goes through a lying-down transition state

with barriers of 1.52 eV from the PBE functional and 1.83 eV from the RBPE functional. Fe(100) is slightly less stable and structurally more open than Fe(110). Both experimental [19,20] and theoretical [28,29] studies have shown that CO favors adsorption on Fe(100) at the ffh site with the molecular axis tilted away from the surface normal by about 50°. Such a binding configuration allows for an increased interaction between the O atom and the Fe surface. As a result, the C–O bond is elongated to 1.320 Å, with an extremely low C–O stretching frequency of 1210 cm^{-1}. In addition, the energy barrier for CO dissociation from this tilted fourfold site at 1/4 ML was predicted to be around 1.1 eV for the PW91 functional. Although Fe(111) is less stable than Fe(110) and Fe(100), it is thought to have high catalytic activity due to its very open structure [62]. Our present work reveals that CO adsorbed at the br site is a precursor for dissociation and has an elongated C–O bond of 1.239 Å. This adsorption state should correspond to the *state a* ($\nu_{C-O} = 1500$ cm^{-1}) reported in TDS and HREELS experiments by Seip et al. [32]. This suggests that the activation of the C–O bond on Fe(111) is stronger than that on Fe(110) but weaker than that on Fe(100). As expected, our predicted RBPE barrier for CO dissociation from the br site at 1/3 ML is 1.53 eV between those of Fe(110) and Fe(100). It indicates that the surface structure of body-centered cubic Fe plays an important role in CO dissociation, with activity toward CO on the order of Fe(100) > Fe(111) > Fe(110).

4. Conclusion

CO dissociation on clean and hydrogen-precovered Fe (111) at a CO coverage of 1/3 ML has been investigated at the level of DFT. It is found that C atoms bind more strongly with Fe(111) than O atoms do. At 1/3 ML, the C atom prefers high coordination sites of the qff (**3/C**) and qp (**4/C**) sites. Comparing the related DFT results reveals that the C atom binds most strongly on Fe(100), followed by Fe (111) and Fe(110). In contrast, the O atom favors the qff (**3/O**) and tsb (**2/O**) sites on Fe(111) and has a different order of adsorption intensity on the low-index Fe surfaces: Fe(111) > Fe(100) > Fe(110).

Starting from the most stable sh site, CO dissociation on clean Fe(111) proceeds stepwise. First, CO diffuses from the most stable sh site to the less stable br site with a 0.20 eV increase in energy, and then dissociates into the C atom at the qp site and the O atom at the qff site in the μ^3 form. The dissociation step has an energy barrier of 1.53 eV and is exothermic by −0.36 eV. The direct dissociation path is not competitive due to its higher barrier of 2.71 eV. In addition, the surface structure of body-centered cubic Fe plays an important role in CO dissociation, with activity toward CO in the order Fe(100) > Fe(111) > Fe(110).

For CO dissociation on hydrogen precovered Fe(111), a new stepwise hydrogen-assisted dissociation mechanism ($CO_{ads} + 2H_{ads} \rightarrow CHO_{ads} + H_{ads}$; $CHO_{ads} + H_{ads} \rightarrow CH_{ads} + O_{ads} + H_{ads}$) has been proposed. First, the dissociatively adsorbed H atom attacks the adsorbed CO forming the CHO species, in which the C–O bond is highly activated by surface Fe. Then the C–O bond is broken, leading to the key FTS intermediates, surface CH and O species. This stepwise path is kinetically most favored, with the lowest energy barrier of 1.17 eV. In contrast, the path $CO_{ads} + 2H_{ads} \rightarrow C_{ads} + O_{ads} + 2H_{ads}$, considered an elementary step in the widely accepted carbide mechanism for FT synthesis [7,8] and the path $CO_{ads} + 2H_{ads} \rightarrow C_{ads} + OH_{ads} + H_{ads}$ suggested by Bianchi and Bennett [38], are not competitive because of their higher energy barriers (1.76 and 1.79 eV, respectively).

Acknowledgments

This work was supported by the National Natural Science Foundation of China (Grants 20473111 and 20590361) and the National Outstanding Young Scientists Foundation of China (Grant 20625620).

References

[1] Z.P. Liu, P. Hu, J. Chem. Phys. 114 (2001) 8244.
[2] R.B. Anderson, The Fischer–Tropsch Synthesis, Academic Press, Orlando, FL, 1984, p. 3.
[3] R.D. Kelly, D.W. Goodman, in: D.A. King, D.P. Woodruff (Eds.), The Chemical Physics of Solid Surfaces and Heterogeneous Catalysis, vol. 4, Elsevier, Amsterdam, 1982, p. 427.
[4] A.T. Bell, Catal. Rev.-Sci. Eng. 23 (1981) 203.
[5] A.J.H.M. Kock, J.W. Geus, Prog. Surf. Sci. 20 (1985) 165.
[6] C.K. Rofer-Depoorter, Chem. Rev. 81 (1981) 447.
[7] F. Fischer, H. Tropsch, Brennstoff Chem. 7 (1926) 97.
[8] R.C. Brady III, R. Pettit, J. Am. Chem. Soc. 102 (1980) 6181.
[9] M. Watanabe, T. Kadowaki, Appl. Surf. Sci. 28 (1987) 147.
[10] G.D. Renshaw, C. Roscoe Jr., P.L. Walker, J. Catal. 18 (1970) 164.
[11] J.P. Reymond, P. Mériaudeau, S.J. Teichner, J. Catal. 75 (1982) 39.
[12] L. Gonzalez, R. Miranda, S. Ferrer, Surf. Sci. 119 (1982) 61.
[13] W. Erley, J. Vac. Sci. Technol. 18 (1981) 472.
[14] G. Wedler, H. Ruhmann, Surf. Sci. 121 (1982) 464.
[15] G. Wedler, H. Ruhmann, Appl. Surf. Sci. 14 (1983) 137.
[16] S.P. Mehandru, A.B. Anderson, Surf. Sci. 201 (1988) 345.
[17] A. Stibor, G. Kresse, A. Eichler, J. Hafner, Surf. Sci. 507–510 (2002) 99.
[18] D.E. Jiang, E.A. Carter, Surf. Sci. 570 (2004) 167.
[19] D.W. Moon, D.J. Dwyer, S.L. Bernasek, Surf. Sci. 163 (1985) 215.
[20] D.W. Moon, S.L. Bernasek, J.P. Lu, J.L. Gland, D.J. Dwyer, Surf. Sci. 184 (1987) 90.
[21] D.W. Moon, S. Cameron, F. Zaera, W. Eberhardt, R. Carr, S.L. Bernasek, J.L. Gland, D.J. Dwyer, Surf. Sci. 180 (1987) L123.
[22] D.W. Moon, S.L. Bernasek, D.J. Dwyer, J.L. Gland, J. Am. Chem. Soc. 107 (1985) 4363.
[23] R.S. Saiki, G.S. Herman, M. Yamada, J. Osterwalder, C.S. Fadley, Phys. Rev. Lett. 63 (1989) 283.
[24] J.P. Lu, M.R. Albert, S.L. Bernasek, Surf. Sci. 217 (1989) A358.
[25] M.H. Nassir, B. Frühberger, D.J. Dwyer, Surf. Sci. 312 (1994) 115.
[26] M.H. Nassir, D.J. Dwyer, P. Kleban, Surf. Sci. 356 (1996) L429.
[27] G. Blyholder, M. Lawless, Surf. Sci. 290 (1993) 155.
[28] D.C. Sorescu, D.L. Thompson, M.M. Hurley, C.F. Chabalowski, Phys. Rev. B 66 (2002) 035416.
[29] T.C. Bromfield, D. Curulla Ferré, J.W. Niemantsverdriet, ChemPhysChem 6 (2005) 254.
[30] D.C. Sorescu, Prepr. Pap.-Am. Chem. Soc. Div. Fuel Chem. 50 (2005) 147.
[31] D. Curulla Ferré, A. Govender, T.C. Bromfield, J.W. Niemantsverdriet, J. Phys. Chem. B 110 (2006) 13897.
[32] U. Seip, M.C. Tsai, K. Christmann, J. Küppers, G. Ertl, Surf. Sci. 139 (1984) 29.
[33] C.E. Bartosch, L.J. Whitman, W. Ho, J. Chem. Phys. 85 (1986) 1052.
[34] L.J. Whitman, L.J. Richter, B.A. Gurney, J.S. Villarrubia, W. Ho, J. Chem. Phys. 90 (1989) 2050.

[35] Y.H. Chen, D.B. Cao, J. Yang, Y.W. Li, J. Wang, H. Jiao, Chem. Phys. Lett. 400 (2004) 35.
[36] E.E. Unmuth, L.H. Schwartz, J.B. Butt, J. Catal. 63 (1980) 404.
[37] S.V. Ho, P. Harriott, J. Catal. 64 (1980) 272.
[38] D. Bianchi, C.O. Bennett, J. Catal. 86 (1984) 433.
[39] M.C. Payne, D.C. Allan, T.A. Arias, J.D. Joannopoulos, Rev. Mod. Phys. 64 (1992) 1045.
[40] V. Milman, B. Winkler, J.A. White, C.J. Pickard, M.C. Payne, E.V. Akhmataskaya, R.H. Nobes, Int. J. Quantum Chem. 77 (2000) 895.
[41] J.P. Perdew, S. Burke, M. Ernzerhof, Phys. Rev. Lett. 77 (1996) 3865.
[42] J.A. White, D.M. Bird, Phys. Rev. B 50 (1994) 4954.
[43] D. Vanderbilt, Phys. Rev. B 41 (1990) 7892.
[44] S.K. Nayak, M. Nooijen, S.L. Bernasek, J. Phys. Chem. B 105 (2001) 164.
[45] H.S. Cheng, D.B. Reiser, S.W. Dean Jr., K. Baumert, J. Phys. Chem. B 105 (2001) 12547.
[46] Q. Ge, S.J. Jenkins, D.A. King, Chem. Phys. Lett. 327 (2000) 125.
[47] T.A. Halgren, W.N. Lipscomb, Chem. Phys. Lett. 49 (1977) 225.
[48] B. Hammer, L.B. Hansen, J.K. Nørskov, Phys. Rev. B 59 (1999) 7413.
[49] J. Sokolov, F. Jona, P.M. Marcus, Phys. Rev. B 33 (1986) 1397.
[50] C.F. Huo, Y.W. Li, J. Wang, H. Jiao, J. Phys. Chem. B 109 (2005) 14160.
[51] G. Herzberg, Molecular Spectra and Molecular Structure. I. Spectra of Diatomic Molecules, Van Norstrand–Reinhold, New York, 1950, p. 521.
[52] M.E. Dry, Catal. Rev. Sci. Eng. 23 (1981) 265.
[53] S.L. Bernasek, M. Zappone, P. Jiang, Surf. Sci. 272 (1992) 53.
[54] R. Burch, A.R. Flambard, J. Catal. 78 (1982) 389.
[55] W.M.H. Sachtler, D.F. Shriver, W.B. Hollenberg, A.F. Lang, J. Catal. 92 (1985) 429.
[56] D.E. Jiang, E.A. Carter, Phys. Rev. B 71 (2005) 045402.
[57] P. Błoński, A. Kiejni, J. Hafner, Surf. Sci. 590 (2005) 88.
[58] Z.P. Liu, P. Hu, J. Am. Chem. Soc. 123 (2001) 12596.
[59] J.B. Benziger, R.J. Madix, Surf. Sci. 94 (1980) 119.
[60] K. Honkala, A. Hellman, I.N. Remediakis, A. Logadottir, A. Carlsson, S. Dahl, C.H. Christensen, J.K. Nørskov, Science 307 (2005) 555.
[61] F. Bozso, G. Ertl, M. Grunze, M. Weiss, Appl. Surf. Sci. 1 (1977) 103.
[62] N.D. Spence, R.C. Schoonmaker, G.A. Somorjai, J. Catal. 74 (1982) 129.